Journal of Korean Society of
Coastal and Ocean Engineers
Vol. 13, No. 1, pp. 46~55, March 2001

Simulation of Wave-Induced Currents by Nonlinear Mild-Slope Equation
비선형 완경사 방정식에 의한 연안류의 모의

Jung Lyul Lee*, Chan Sung Park**, and Sang Woo Han*
이정렬* · 박찬성** · 한상우*

Abstract □ An approach using the nonlinear wave model in predicting wave-induced currents is presented. The model results were compared with those of the conventional model using phase-averaged radiation stress, and in addition with experimental data captured by a PIV system. As a result of comparison of wave-induced currents generated behind the surface-piercing breakwater and submerged breakwater, eddy patterns appeared to be similar each other but in general numerical solutions of both models were underestimated.

Keywords : PIV, Wave-Induced Currents, Nonlinear Wave Model, Mild-Slope Equation, Radiation Stress

要 旨 : 비선형 파랑 모형을 이용하여 해안류를 산정하는 모형이 소개되었다. 기존의 잉여응력을 이용한 수치모형 결과와 비교하였으며, 두 수치모형의 타당성 검토를 위하여 PIV 시스템으로 획득한 실험자료와도 비교하였다. 방파제 및 잠제 후면에서 형성되는 해안류에 대하여 서로 비교한 결과, 소용돌이 흐름의 형태는 유사하나 관측 결과와 비교하여 수치 모형 결과가 대체로 과소평가되고 있다.

핵심용어 : PIV, 해안류, 비선형파 모형, 완경사 방정식, 잉여응력

1. INTRODUCTION

The nearshore currents are required for the preservation of coastal areas and the more pressing environmental problems since they are the major forces for sediments to be in suspension and transport the sediments into tranquil regions. Numerical models are often used to calculate current patterns formed around man-made or naturally caused changes around coastal area. A prominent feature in the nearshore zone is the wave-induced current circulation. Two classes of approaches exist to simulate such wave-induced currents: (i) phase-averaged models that calculate large scale motions due to wave-induced forcing and (ii) models that resolve the instantaneous state of motion, such as models based on the nonlinear mild slope equations or the Boussinesq equations.

1.1 Phase-Averaged Approach

It is commonly accepted that the primary driving force for phase-averaged currents is gradients in the radiation stresses first introduced by Longuet-Higgins and Stewart (1961), which are defined as the excess momentum flux due to wave motion. The basic equations of mass and momentum are obtained through phase-averaged and depth-integrated approach, and its modeling has advanced considerably from the earlier development by Noda *et al.* (1974) and Ebersole and Dalrymple (1979). Both of these earlier models were driven by a wave refraction model with no current feedback. In recent years, Yoo and O'Connor (1986) developed a coupled wave-induced circulation model based upon what could be classified as a hyperbolic type wave equation; Yan (1987) and Winer (1988) developed their interaction models based upon parabolic approximation of the wave equation. All these models employed the depth-averaged or depth-integrated formulations. Recently, some models for determining the three dimensional currents have been proposed. De Vriend and Stive (1987), Lee (1993), and Kuroiwa *et al.*

*성균관대학교 토목환경공학과(Dept. of Civil and Environmental Eng., Sungkyunkwan University, Suwon Campus, Suwon 440-746, Korea)
**(주)도화종합기술공사 항만부(Dept. of Port and Coast Eng., Dohwa Consulting Engineers Co., Ltd. Seoul 135-780, Korea)

(1998) improved the nearshore circulation model by employing a quasi-three dimensional technique. This technique is very attractive to accommodate the surf zone in which the depth-averaged model is no longer valid. For the three dimensional nearshore currents, some models (Pechon and Teisson, 1994; Nobuoka *et al.*, 1998) also have been developed in the surf zone. The Nobuoka's 3D model was developed by using the vertical distribution of radiation stresses.

1.2 Nonlinear Wave Approach

The conventional models for wave-induced currents are based on a splitting of the phenomenon into a linear wave problem described by the mild-slope equation and a current problem described by the shallow water equations including radiation stress. Wave-current interaction effects such as current-induced refraction and wave blocking may be included in these systems by successive and iterative model executions.

More recently, however, a more direct approach to the problem has been proposed by Kabiling and Sato (1993) and Sorensen *et al.* (1994). The approach is accomplished by the use of a Boussinesq model which automatically includes the combined effects of wave-wave and wave-current interaction without need for inclusion of radiation stress. It is notable that the approach of using the radiation stress has the major restriction on the reflected wave existing condition since the conventional radiation stresses can be derived under the progressive wave field.

2. DIRECT PREDICTION BY NONLINEAR MILD-SLOPE EQUATION

A set of weakly nonlinear wave equations has been derived by Lee and Park (2000) with inclusion of nonlinear terms in derivation of the mild-slope equation (Berkhoff, 1972). In the present study, the equation set is used as a dispersive wave-current model:

$$\frac{\partial^2\eta}{\partial t^2}+\nabla\cdot\left[\left(\frac{CC_g}{g}+\eta\right)\left(\frac{\partial \boldsymbol{u}_o}{\partial t}\right)\right]+\nabla\cdot\left(\boldsymbol{u}_o\frac{\partial\eta}{\partial t}\right)+\frac{\sigma^2-k^2CC_g}{g}\left[\frac{1}{2}\boldsymbol{u}_o^2+g\eta+\eta\frac{\partial^2\eta}{\partial t^2}+\frac{1}{2}\left(\frac{\partial\eta}{\partial t}\right)^2\right]=0 \quad (1)$$

$$\frac{\partial \boldsymbol{u}_o}{\partial t}+g\nabla\eta+\boldsymbol{u}_o\cdot\nabla\boldsymbol{u}_o+\frac{3}{2}\nabla\left(\frac{\partial\eta}{\partial t}\right)^2=0 \quad (2)$$

where η is the free surface displacement, $\boldsymbol{u}_o$ the horizontal velocity vector defined at the mean water level, C and C_g are the local phase speed and the group velocity, respectively, g the gravitational acceleration, k the wave number, and σ the angular frequency. $\tau_B = F_{bf}|u_{orb}|u_{orb}$ where F_{bf} is the friction coefficient, and $|u_{orb}|$ is given by $gH/2C\cosh kh$.

Equation (1) has been derived by using the Galerkin's method; that is, taking depth-integration after multiplying the vertical structure function on a continuity equation, while Eq.(2) has been obtained by simply taking the horizontal differentiation on Bernoulli equation at the mean water level.

The governing equations (1) and (2) are solved by using a fractional step method in conjunction with the approximate factorization techniques leading to the implicit finite difference schemes. It turns out that the implicit scheme accelerates the convergence of numerical calculations for the steady-state solutions. We used the Miche's criterion (Miche, 1951) as the breaking wave model because it is simple and accurate enough, and guarantees stability. For the mass conservation, the broken volume due to wave breaking is consequently passed on the next step elevation at each grid.

3. PHASE-AVERAGED APPROACH

The second model is based on results obtained by Lee and Wang (1993) in the depth-integrated form. The continuity equation:

$$\frac{\partial\eta_c}{\partial t}+\frac{\partial}{\partial x}(Q_x+M_x)+\frac{\partial}{\partial y}(Q_y+M_y)=0 \quad (3)$$

where η_c is the mean water level, Q_x and Q_y are the x and y components of the mean flow rate integrated from bottom to mean water level, respectively, as defined below;

$$Q_x=\int_{-h}^{\eta_c}u\,dz \quad \text{and} \quad Q_y=\int_{-h}^{\eta_c}v\,dz$$

where u and v are the x and y components of velocity vector, h is the water depth and M_x and M_y are the phase-averaged flow rate induced by the wave motion, which are evaluated as

$$M_x=\frac{gH^2k_x}{8\sigma} \quad \text{and} \quad M_y=\frac{gH^2k_y}{8\sigma}$$

In the steady state, the depth-integrated total mass flux has to be zero.

The x-directional modified momentum equation:

$$\frac{\partial Q_x}{\partial t}+\frac{\partial}{\partial x}\left(\frac{Q_x^2}{h+\eta_c}\right)+\frac{\partial}{\partial y}\left(\frac{Q_xQ_y}{h+\eta_c}\right)+\frac{1}{\rho}\frac{\partial S_{xx}}{\partial x}+\frac{1}{\rho}\frac{\partial S_{yx}}{\partial y}+g(h+\eta_c)\frac{\partial \eta_c}{\partial x}+\frac{\tau_{Bx}}{\rho}=0 \quad (4)$$

The y-directional modified momentum equation:

$$\frac{\partial Q_y}{\partial t}+\frac{\partial}{\partial x}\left(\frac{Q_xQ_y}{h+\eta_c}\right)+\frac{\partial}{\partial y}\left(\frac{Q_y^2}{h+\eta_c}\right)+\frac{1}{\rho}\frac{\partial S_{xy}}{\partial x}+\frac{1}{\rho}\frac{\partial S_{yy}}{\partial y}+g(h+\eta_c)\frac{\partial \eta_c}{\partial y}+\frac{\tau_{By}}{\rho}=0 \quad (5)$$

where ρ is the water density,

$$S_{xx}=E\left[n(\cos^2\theta+1)-\frac{1}{2}\right]$$

$$S_{xy}=S_{yx}=E[n\sin\theta\cos\theta]$$

$$S_{yy}=E\left[n(\sin^2\theta+1)-\frac{1}{2}\right]$$

where n is the ratio of the group velocity C_g to the phase speed C, and E is the wave energy defined as $\rho gH^2/8$. The bottom friction consists of friction modules due to viscous and streaming flows:

$$\tau_B=\overline{\tau_{B,bf}}+\overline{\tau_{B,strm}}=|u_{orb}|(F_{bf}U_B+F_{strm}U_{strm}) \quad (6)$$

where, F_{bf} is the bottom friction factor, while F_{strm} is the friction factor due to the streaming flow. And $|u_{orb}|=gH/2C\cosh kh$ as the orbital velocity at the bottom, U_B is the current velocity at the bottom level, and U_{strm} is the streaming current measured at the bottom under progressive waves.

The lateral shear stress is added to the momentum equation as

$$\tau_l=-\rho\left[\varepsilon_y\frac{\partial u}{\partial y}+\varepsilon_x\frac{\partial v}{\partial x}\right] \quad (7)$$

The mixing length coefficient, ε_x is assumed to be constant here for the practical use, instead of values proportional to the distance from the shoreline, $|x|$.

The wave properties such as wave height, wave angle, phase speed and group velocity shown above are computed by the linear wave model described briefly here. As done by Madsen and Larsen (1987) for the regular waves, a hyperbolic equation set obtained based on Smith and Sprinks (1975) was reformulated extracting the harmonic time variation with letting $\eta = S\exp(-i\sigma t)$ and $\boldsymbol{u}_o = \boldsymbol{U}_o\exp(-i\sigma t)$:

$$\frac{\partial^2 S}{\partial t^2}-2i\sigma\frac{\partial S}{\partial t}+\nabla\cdot\left[\frac{CC_g}{g}\left(\frac{\partial U_o}{\partial t}-i\sigma U_o\right)\right]-k^2CC_gS=S_S \quad (8)$$

$$\frac{\partial U_o}{\partial t}-i\sigma U_o+g\nabla S=0 \quad (9)$$

This approach speeds up the solution considerably since one does not need to resolve the wave period any longer. The source term S_s which generates the incoming wave is given in terms of the internal wave condition S_I on the grid mesh of $\Delta x\times\Delta y$:

$$S_S=2\sigma C_gS_I\frac{\Delta s}{\Delta x\Delta y} \quad (10)$$

where $S_I=\frac{H_I}{2}\exp(i\int k\cos\theta_I dx+i\int k\sin\theta_I dy)$, Δs is the width of the wave front inside a grid mesh, S_I is the height function of internal waves, H_I is the wave height, and θ_I is the wave direction. For the treatment of boundary condition, Lee(2001)'s approach was taken rather than the sponge layer approach.

The governing equations (3), (4) and (5) are also solved by using a fractional step method in conjunction with the approximate factorization techniques leading to the implicit finite difference schemes. The mild slope equations (8) and (9) are also solved by the same approximate factorization techniques in which complex variable are used for effective calculations of wave height and wave angle. The Miche's criterion (Miche, 1951) as used in the first approach was also used for simulating the wave breaking process.

4. PIV EXPERIMENTS

Most of former experimental works were focused on the measurement of the water surface displacements without taking the flow patterns around the obstacle into account. Although it was expected that a man-made structure permits the nearshore circulation, it was rarely measured how strong currents can be induced around it, particularly in the case of breaking waves. Recently, a

several image-based system allows to visualize the flow field near a breakwater with detailed information about the flow distributions.

4.1 PIV

Particle Image Velocimetry(PIV) is a superior flow visualization technique for providing an instantaneous, non-intrusive insight into velocity field distributions with qualitative and quantitative information. It offers many advantages over other conventional velocimetries, such as laser Doppler anemometry and hot-wire anemometry.

PIV principals are as follows. Firstly, the flow field plane section of a flow containing neutrally buoyant particles is illuminated, typically by laser light. And then illuminated particles within flow field are captured by CCD camera or camcorder. Finally, an image analysis technique is used to determine the particle displacements in time interval of sequential images to visualize the velocity field.

Basic concept of PIV is a comparison of two successive images during small interval time, Δt are divided into small area called interrogation area and searching area as shown in Fig. 1. Interrogation and searching area are compared in the two successive images using the cross correlation algorithm. The Cross Correlation PIV assumes the velocity relatively uniform within a search region and no change in the flow pattern between two successive images. PIV has restrictive spatial resolution because velocities are assumed uniform within interrogation area. A spatial shift caused by the fluid flow may be observed from interrogation area to the searching area. Generally a side length of searching area, M is a little larger than the drift by the greatest velocity in the whole flow field.

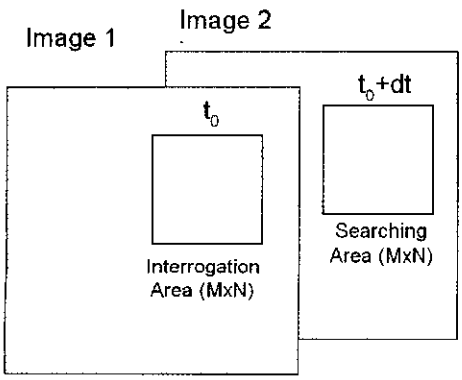

Fig. 1. Interrogation area and searching area.

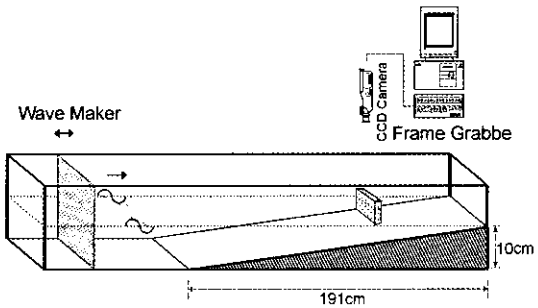

Fig. 2. Schematic description of the experimental setup.

4.2 PIV Setup

A schematic description of the experiment setup is shown in Fig. 2, which consists of wave deformation system and image capturing system. The fluid velocity was obtained using optical and digital processing techniques. While the image processing algorithm employed herein is similar to conventional PIV, special consideration is needed for particle size and flow tracing. Under the wave breaking, the wave-induced turbulent flow motion was strongly generated in surf zone so that the plastic balls of about 5 mm diameter, which is relatively large size than conventional particle size, were used to exclude the small-scaled turbulent motion. For the illumination under the sunlight, white-colored balls were used.

The displacement fields were recorded by a SMD-1M60 CCD camera (SMD co.) with a 50 mm Nikkor lens (Nikon Co.). The image data were stored digitally using an AM-MTD (Imaging Technology) frame grabber, set to record the gray-level images from the CCD camera. To extract current velocity distributions from the successive images, Matlab by the MathWorks Inc., a manipulation software package, was used to process the images on the Pentium Personal Computer. In undertaking the PIV experiments, flow images of 1024×1024 pixels were taken in 1/13 sec interval, and the interrogation area of 128×128 pixels was used. The scanned area corresponds to a square region 896×1024 pixel.

4.3 Experimental Setup

In order to evaluate the capabilities of the numerical model, computations will be compared with the physical experiments carried out in this study. The experiment was

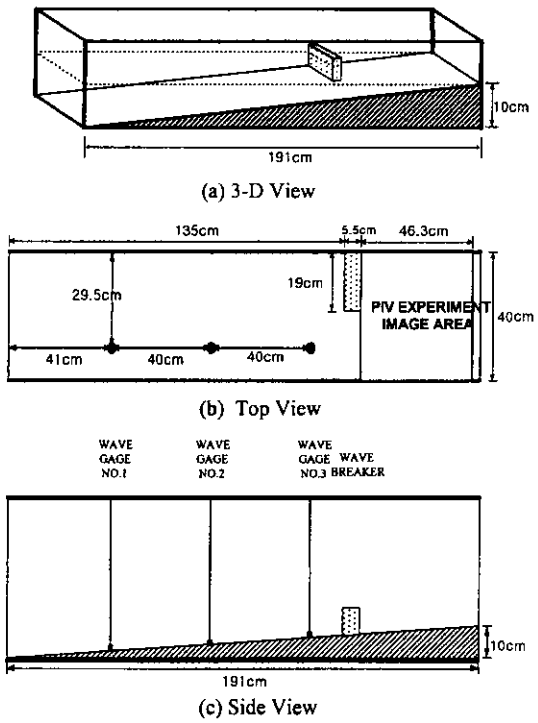

Fig. 3. Physical layout of experiment of Case 1: (a) 3-D view, (b) top view, (c) side view.

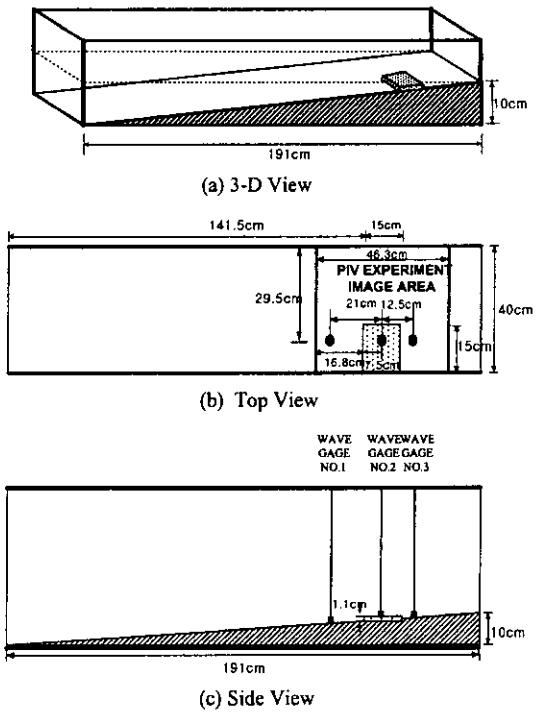

Fig. 4. Physical layout of experiment of Case 2: (a) 3-D view, (b) top view, (c) side view.

conducted in a Coastal-Hydraulics Laboratory wave flume of Sungkyunkwan University, in order to verify the numerical results of wave-induced currents. The wave flume of 50 cm deep, 40 cm wide, and 12 m long consists of a wave generator and beach zones. The bottom and side walls of the flume are glass to allow easy optical access. The regular waves were generated by a piston-type wave paddle and the beach slope of 1/19 was set at the other end of the wave flume.

Physical experiments were accomplished for two cases. Experimental conditions are same for two different experimental setups; $T = 0.8$ sec, $H_i = 2$ cm, U_r(Ursell parameter)=10.05 and H_i/L(wave steepness)=0.0282. The layouts of two different experimental configurations are illustrated in Figs. 3 and 4 showing the locations of the measurement stations and detailed geometry of the flume. The exposed breakwater was placed to the left half of the wave tank looking in the direction of the wave propagation, while the submerged breakwater was placed to the left side.

The wave flume was decorated with the data acquisition system to conform the incident wave height and to access the wave profiles from the wave gages. Gages were connected with amplifier for increasing analog signals. Then the DaqBoard 100A (DaqBoard), A/D converter, changes conditioned signals into corresponding digital numbers saved as ASCII format.

For the Case 1 as shown in Fig. 3, wave gages 1, 2 and 3 were located at x=41 cm, x=81 cm and x=121 cm measured shoreward from the toe of slope, respectively. The measuring line was located about 10.5 cm apart from the nearer sidewall. The Case 2 for the submerged breakwater are as shown in Fig. 4. Wave gages 1, 2 and 3 were located at x=−21.5 cm, x=0 cm (center) and x=12.5 cm measured shoreward from the center of submerged breakwater, respectively. The submerged breakwater of area 15×15 cm^2 is impermeable and 1.1 cm high.

5. NUMERICAL RESULTS AND COMPARISON WITH PIV EXPERIMENTS

As an example of the capability of PIV system, the

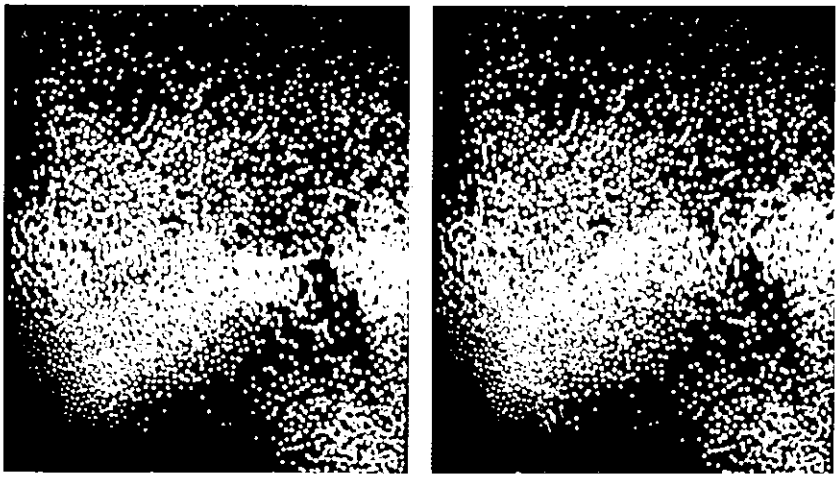

Fig. 5. Particle image taken in 1/13 sec interval under the wave condition of H_i=2 cm, and T=0.8 s, Case 1 (threshold level 70 given).

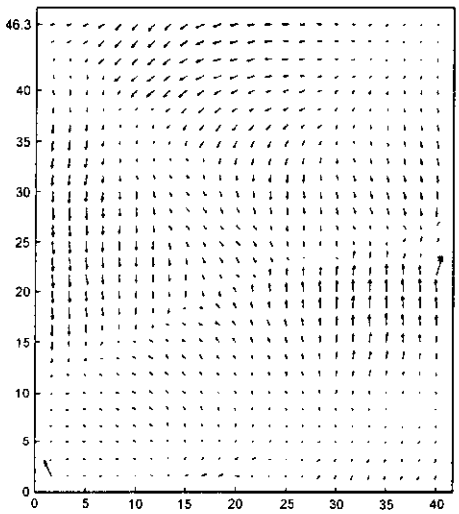

Fig. 6. Instantaneous velocity vectors obtained from two successive images in Fig. 5.

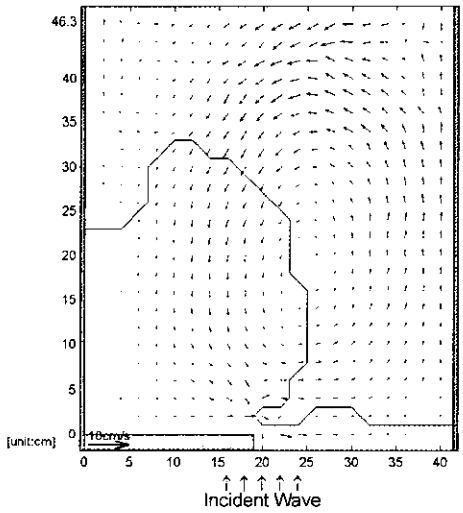

Fig. 7. Current vectors by the nonlinear wave model for Case 1 (solid line: breaking line).

distribution of instantaneous vectors is presented for one of the physical experiments carried out in this study. The two successive images shown in Fig. 5 are taken in 1/13 *sec* interval by CCD camera under the wave condition of H_i = 2 cm, and T = 0.8 s, and the resulting velocity vectors are plotted in Fig. 6. The threshold level used for image treatment was 70.

Current vectors of Case 1 resulted from both nonlinear wave phase approach and phase-averaged radiation stress approach, and PIV experiments were compared on the image size as shown in Figs. 7-9, respectively. The radiation stress approach was done with no current feedback. An observed image area is of 40 cm width and 46.3 cm length as shown in Fig. 3. The computational grid domain was chosen to cover the whole plan-form area of the wave flume tank and consisted of 120×22 grid points, of uniform grid spacing of 2 cm. At the open boundary, water elevations were prescribed by a sine wave. Time-steps were differently applied according to the models; 0.015 sec was used for phase-resolving nonlinear model and 0.15 sec for phase-averaged radiation stress model. The nonlinear wave phase model and the experimental

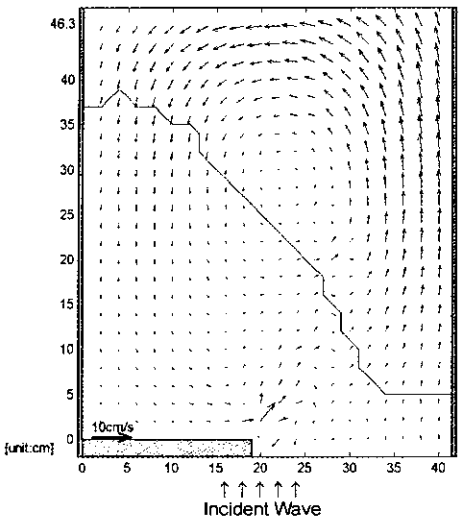

Fig. 8. Current vectors by the radiation stress model of Case 1 (solid line: breaking line).

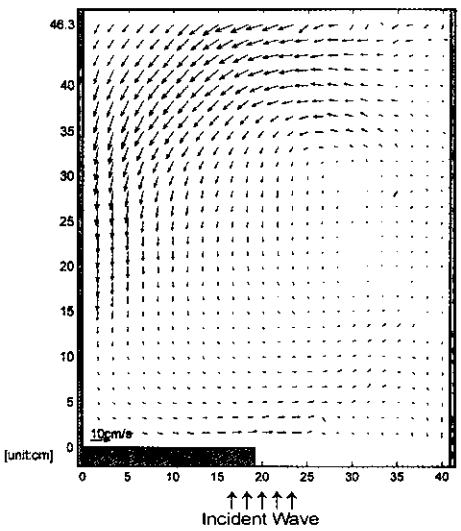

Fig. 9. Current vectors by physical experiments of Case 1.

data were time-averaged over last several wave periods. Both side boundaries on the image are impermeable glass wall but the upwave and downwave boundaries are open so as to permit vectors crossing with them.

The breaking lines are also simultaneously shown with current vectors in model results. The breaking line in physical experiments was hard to be recognized. It is found in all Figs of Case 1 that a closed eddy flow is generated behind the breakwater. As shown in Figs. 7 and 8, both model results show good agreement each other.

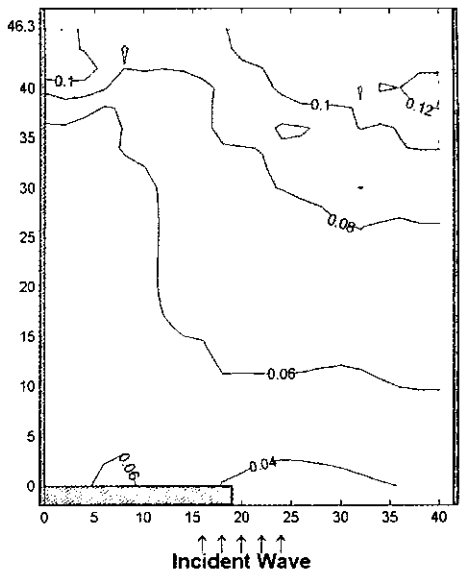

Fig. 10. Normalized set-up contours by the nonlinear wave model of Case 1.

However, the observed results show overall agreement in circulation pattern with model results but as shown in experiments by PIV system (Fig. 9) the strong seaward currents behind a breakwater do not appear in both model results. The major difference is thought to happen since both models do not take into account the strong shoreward volume flux cast near crest levels as waves break. Therefore, such effect should be taken into account for better accuracy. As shown in Fig. 9, the current vectors depicted by PIV experiments seem to fail in the mass balance in a control volume though the overall performance is satisfactory. The primary reason is thought that the image capturing time interval is not enough to keep up with the fast moving shoreward orbital motions.

The spatial variations of normalized set-up from both models are compared in Figs. 10-11. The set-up was normalized by the incident wave height. The computed distribution shows quite different results. Results by nonlinear wave model provided set-ups of positive values in the domain shown in the Fig., while those by radiation stress model provided set-downs of negative value in the right-lower region. Another significant discrepancy is that an isolated set-up contour of 0.06 was formed right behind the breakwater in nonlinear wave model results.

The experiments are also performed for a submerged breakwater. Two models and one PIV experiment (Case 2)

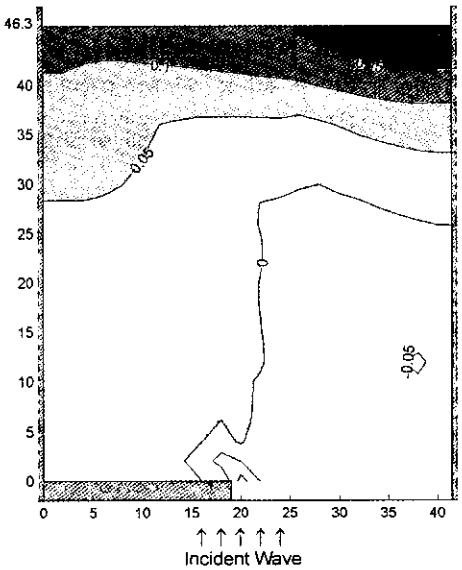

Fig. 11. Normalized set-up contours by the radiation stress model of Case 1.

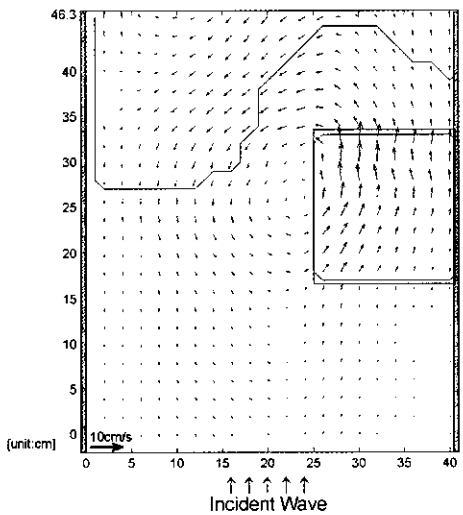

Fig. 12. Current vectors by the nonlinear wave model of Case 2 (solid line: breaking line).

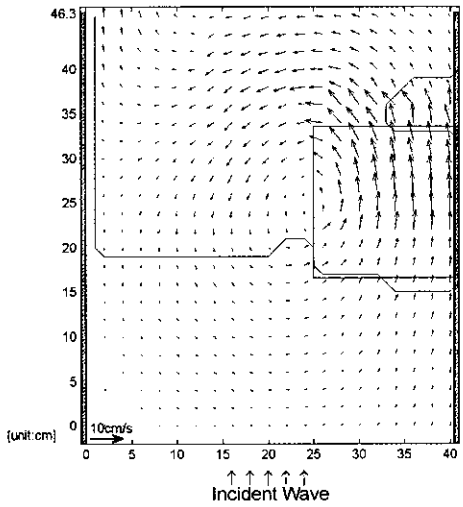

Fig. 13. Current vectors by the radiation stress model of Case 2 (solid line: breaking line).

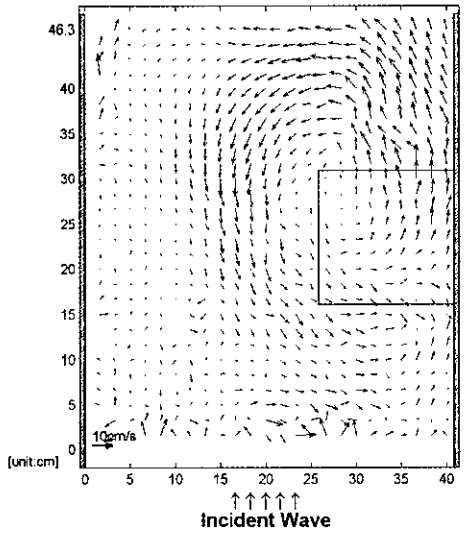

Fig. 14. Current vectors by physical experiments of Case 2.

were also carried out. The results for current pattern are shown in Figs. 12-14, respectively. In undertaking the numerical model tests, the same computing conditions as those of the Case 1 were given. The computed breaking lines indicated as solid lines appeared similar each other but the re-breaking line by nonlinear wave model was resulted wider and shallower than that by the radiation stress model. PIV measurements show that the onshore currents over a submerged breakwater are still underestimated when compared with both model results and eye observation.

The spatial variations of normalized set-up are shown in Figs. 10-11. Radiation stress model provided the sharp increment of set-up after breaking process, whereas the nonlinear wave model did provide the mild increment. This fact might be mainly due to the re-breaking process of waves behind a submerged breakwater as compared in Figs. 12 and 13.

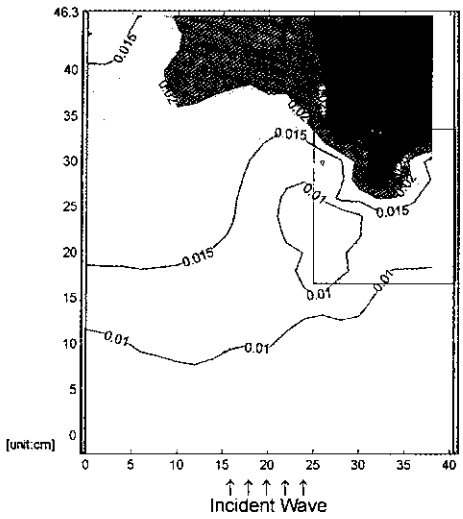

Fig. 15. Normalized set-up contours by the nonlinear wave model of Case 2.

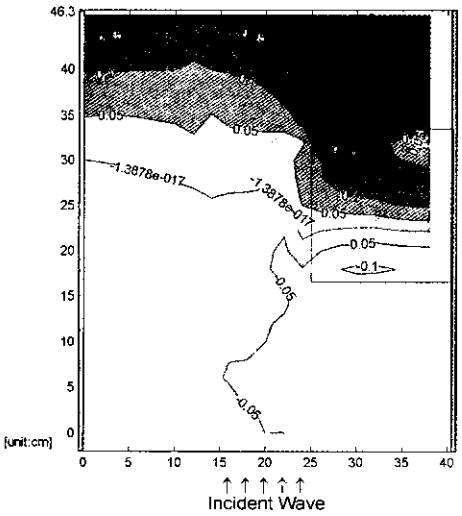

Fig. 16. Normalized set-up contours by the radiation stress model of Case 2.

6. CONCLUSIONS

Comparison was accomplished for three kinds of results from nonlinear wave phase approach and phase-averaged radiation stress approach, and PIV experiments. The wave-induced currents in nonlinear wave phase approach were determined by integrating the depth-integrated velocities over wave periods and then dividing it by the number of wave period taken and the local mean water depth. In the present study for comparison, the phase-averaged radiation stress approach was done with no current feedback.

Results from both models showed reasonable agreement each other although the input parameters such as breaking criterion and mixing condition could not be given same values. As compared with the observed results, both numerical approaches provided the underestimated strength of current vectors.

We offered the erroneous physical results to show the limitation of the present PIV technique that could be overcome by the mechanical choking to shorten the time interval, or hardware/software in the further for accessing images in shorter interval. Another weakness in the present PIV measurement is that the mean positions of particles used for the image capture were observed biased to the bottom due to little higher specific gravity than unit.

ACKNOWLEDGEMENT

This work has been funded partly by the Wave Monitoring Program of Ministry of Maritime Affairs & Fisheries. The authors appreciate Dr. D.Y. Lee, KORDI for his support and suggestion.

REFERENCES

Berkhoff, J.C.W., 1972. Computation of combined refraction-diffraction, *Proc. 13rd Int. Conf. Coastal Engrg.*, ASCE, 471-490.

De Vriend, H.J., and Stive, M.J.F., 1987. Quasi-3D modeling of nearshore currents, *Coastal Engrg.*, **11**, 565-601.

Ebersole, B.A., and Dalrymple, R.A., 1979. A numerical model for nearshore circulation including convective accelerations and lateral mixing, Ocean Engineering Report No. 21, Dept. of Civil Eng., Univ. of Delaware, Newark, Delaware.

Kabiling, M.B., and Sato, S., 1993. Two-dimensional nonlinear dispersive wave-current and three-dimensional beach deformation model, *Coastal Engrg. in Japan*, **36**, 196-212.

Kuroiwa, M., Noda, H., and Matsubara, Y., 1998. Application of a quasi-three dimensional numerical model to nearshore currents, *Proc. 26th Int. Conf. Coastal Engrg.*, ASCE, 815-828.

Lee, J.L., 1993. Wave-current interaction and quasi-three-dimensional modeling in nearshore zone, Ph.D dissertation,

Coastal and Oceanographic Engineering Department, Univ. of Florida, Gainesville.

Lee, J.L. and Park, C.S., 2000. Development of Weakly Nonlinear Wave Model and Its Numerical Simulation, *J. the Korean Society of Coastal and Ocean Engineers*, **12**(4), 181-189.

Lee, J.L. and Wang, H., 1993. Mathematical model for 3-dimensional circulation in surf zone, *J. the Korean Society of Coastal and Ocean Engineers*, **5**(4), 369-383.

Lee, K.J., 2001. The effect of surface-piercing thin breakwater to harbour tranquility, Master's thesis, Department of Civil and Environmental Engineering, Sungkyunkwan Univ., Seoul, Korea.

Longuet-Higgins, M.S., and Stewart, R.W., 1961. The changes in amplitude of short gravity waves on steady non-uniform currents, *J. Fluid Mech.*, **10**, 529-549.

Madsen, P.A., and Larsen, J., 1987. An efficient finite-difference approach to the mild-slope equation, *Coastal Engrg.*, **11**, 329-351.

Miche, R., 1951. The reflecting power of maritime works exposed to action of the waves, Annals of the Highway Dept., National Press, France.

Nobuoka, H., Mimura, N., and Kato, H., 1998. Three-dimesional nearshore currents model based on vertical distribution of radiation stress, *Proc. 26th Int. Conf. Coastal Engrg.*, ASCE, 829-842.

Noda, D., Sonu, C.J., Rupert, V.C., and Collins, J.I., 1974. Nearshore circulation under sea breeze conditions and wave-current interactions in the surf zone, Tetra Tech Report TC-149-4.

Pechon, P., and Teisson C., 1994. Numerical modeling of three-dimensional wave-driven currents in the surf-zone, *Proc. 24th Int. Conf. Coastal Engrg.*, ASCE, 2503-2512.

Sorensen, O.R., Schäffer, H.A., Madsen, P.A., and Deigaard, R., 1994. Wave breaking and induced nearshore circulations, *Proc. 24th Int. Conf. Coastal Engrg.*, 2583-2594.

Yan, Y., 1987. Numerical modeling of current and wave interaction on an inlet-beach system, Techincal Report No. 73, Coastal and Oceanographic Engineering Department, Univ. of Florida, Gainesville.

Yoo, D., and O'Connor, B.A. 1986. Mathematical modeling of wave-induced nearshore circulations, *Proc, 20th Int. Conf. Coastal Engrg.*, ASCE, 1667-1681.

Winer, H.S., 1988. Numerical modeling of wave-induced currents using a parabolic wave equation, Ph.D dissertation, Coastal and Oceanographic Engineering Department, Univ. of Florida, Gainesville.